How to cite: Angew. Chem. Int. Ed. 2024, e202410799
doi.org/10.1002/anie.202410799

Enzyme Catalysis

Isofunctional but Structurally Different Methyltransferases for Dithiolopyrrolone Diversification

Li Su, +[a]Eva M. Huber+, Margaretha Westphalen, Jonas Gellner, Edna Bode, Tania Köbel, Peter Grün, Mohammad M. Alanjary, Timo Glatter, Katarina Cirnski, Rolf Müller, Daniel Schindler, Michael Groll, and Helge B. Bode**

Abstract: Dithiolopyrrolone (DTP) natural products are produced by several different bacteria and have potent antibacterial, antifungal and anticancer activities. While the amide of their DTP core can be methylated to fine-tune bioactivity, the enzyme responsible for the amide *N*-methylation has remained elusive in most taxa. Here, we identified the amide methyltransferase XrdM that is responsible for xenorhabdin (XRD) methylation in *Xenorhabdus doucetiae* but encoded outside of the XRD gene cluster. XrdM turned out to be isofunctional with the recently reported methyltransferase DtpM, that is involved in the biosynthesis of the DTP thiolutin, although its X-ray structure is unrelated to that of DtpM. To investigate the structural basis for ligand binding in both enzymes, we used X-ray crystallography, modeling, site-directed mutagenesis, and kinetic activity assays. Our study expands the limited knowledge of post-non-ribosomal peptide synthetase (NRPS) amide methylation in DTP biosynthesis and reveals an example of convergent evolution of two structurally completely different enzymes for the same reaction in different organisms.

Introduction

Xenorhabdins (XRDs) are members of the dithiolopyrrolone (DTP) class of natural products (Figure S1a). DTPs exhibit broad-spectrum bioactivity against a variety of organisms, including Gram-positive and Gram-negative bacteria, fungi, and even eukaryotic parasites.[1] They share the bicyclic dithiolopyrrolone scaffold, which is biosynthesized by a non-ribosomal peptide synthetase (NRPS) from two cysteine building blocks followed by cyclization, decarboxylation and oxidation (Figure S1b).[2] Tailoring enzymes, such as amino acyltransferases and amide *N*-methyltransferases (MTs), further expand the structural diversity of DTPs, which according to their modifications can be grouped into three subfamilies: *N*-acyl-DTPs (e.g. holomycin), *N*-acyl, *N*-methyl-DTPs (e.g. thiolutin), and thiomarinol, a distinct type carrying the polyketide antibiotic marinolic acid as the *N*-acyl group linked to DTP (Figure S1a).[3]

To date, only thiolutin and derivatives thereof (e.g. aureothricin), as well as a few members of XRDs, such as XRD-243Me, XRD-271Me, XRD-285Me, and XRD-299Me (referring to *N*-methylated XRDs in the following) were

[*] E. Bode, T. Köbel, P. Grün, H. B. Bode
Department of Natural Products in Organismic Interactions, Max Planck Institute for Terrestrial Microbiology, 35043 Marburg, Germany
E-mail: helge.bode@mpi-marburg.mpg.de

+. M. Huber,+ J. Gellner, M. Groll
Technical University of Munich, TUM School of Natural Sciences, Department of Bioscience, Center for Protein Assemblies, 85748 Garching, Germany
E-mail: michael.groll@tum.de

M. Westphalen, H. B. Bode
Molecular Biotechnology, Department of Biosciences, Goethe University Frankfurt, 60438 Frankfurt am Main, Germany

M. M. Alanjary
Bioinformatics Group, Wageningen University, Droevendaalsesteeg 1, Wageningen, PB 6708, Netherlands

T. Glatter
Core Facility for Mass Spectrometry & Proteomics, Max Planck Institute for Terrestrial Microbiology, 35043 Marburg, Germany

K. Cirnski, R. Müller
Helmholtz Institute for Pharmaceutical Research Saarland (HIPS), Helmholtz Centrefor Infection Research(HZI), Saarland University, 66123 Saarbrücken, Germany

K. Cirnski, R. Müller
German Center for Infection Research (DZIF), Partner Site Hannover, 38124 Braunschweig, Germany

T. Köbel, D. Schindler
Max Planck Biofoundry MaxGENESYS, Max Planck Institute for Terrestrial Microbiology, 35043 Marburg, Germany

H. B. Bode
Chemical Biology, Department of Chemistry, Philipps University of Marburg, 35043 Marburg, Germany

H. B. Bode
Senckenberg Gesellschaft für Naturforschung, 60325 Frankfurt am Main, Germany

H. B. Bode
Center for Synthetic Microbiology (SYNMIKRO), University of Marburg, 35043 Marburg, Germany

[+] These authors contributed equally

identified as naturally occurring *N*-acyl, *N*-methyl-DTPs (Figure 1a and Figure S1a). In analogy to holomycin and thiolutin, which differ only in the *N*-methyl group at the endocyclic amide nitrogen position, there are non-methylated and *N*-methylated XRDs with different bioactivities (Table S1), implying that the bioactivity of DTPs is modulated among other things by the amide methyl group.[4]

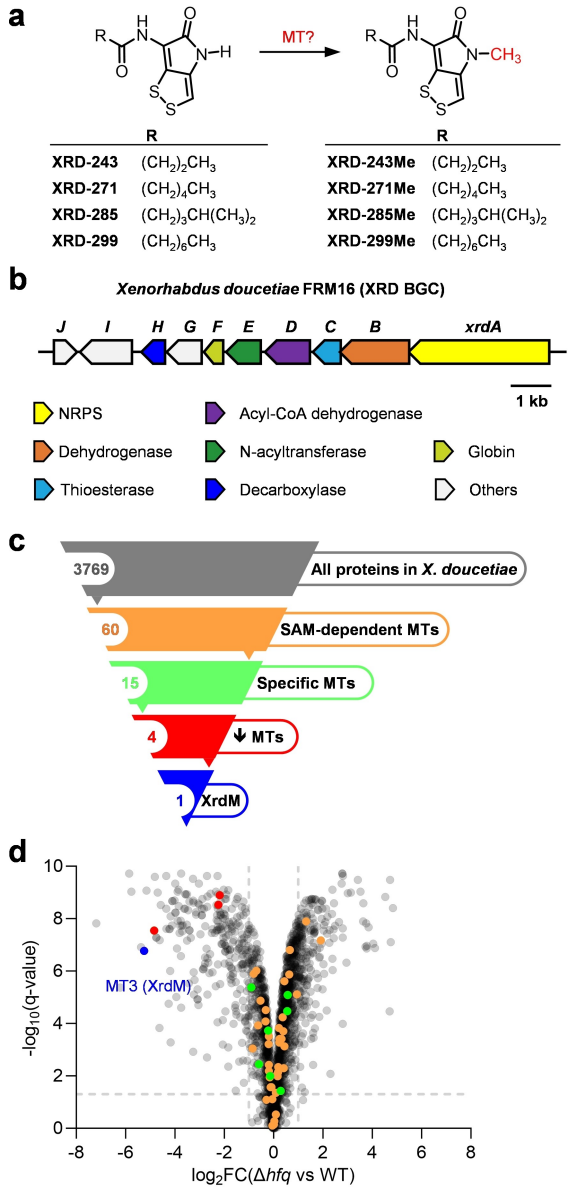

Figure 1. Identification of the XRD *N*-methyltransferase in *X. doucetiae*. **a**) Structures of naturally produced non-methylated and *N*-methylated XRDs with the *N*-methyl moiety highlighted in red. **b**) Biosynthetic gene cluster of XRD in *X. doucetiae* FRM16 lacking an *N*-methyltransferase. **c**) Screening funnel for the identification of the XRD-specific *N*-methyltransferase. Based on bioinformatics selection criteria, 15 MT candidates were examined in overexpression experiments, of which 4 were further checked by gene deletion. Only XrdM was found to be responsible for the *N*-methylation of XRDs. **d**) Volcano plot of the comparative proteomics analysis between the *X. doucetiae* Δ*hfq* mutant and its wild type (WT). Dashed lines show cutoff values q = 0.05, and FC (fold change) = 2. Dots in blue, red, green, and orange refer to MTs according to the screening funnel shown in (**c**). Among them, the green and red dots were MTs specific for *X. doucetiae* (Figure S4) and thus were chosen for an expression test in △*hfq* P_{BAD}_xrdA. The blue (MT3 or XrdM) and red dots were down-regulated MTs that were tested by gene deletion in WT, respectively. Data were calculated from four biological replicates. Detailed information is given in Figure S5.

Usually, methylated non-ribosomal peptides (NRPs) are generated either by using methylated amino acids as building blocks[5] or by methylating the peptides during or after biosynthesis of the scaffold. The latter can be accomplished by MT domains within NRPSs[6] or by individual MTs within the corresponding biosynthetic gene cluster (BGC).[7] However, also MTs encoded outside the corresponding BGC can be engaged in tailoring reactions. Prominent examples are the *S*-MT from gliotoxin biosynthesis[8] and the *N*-MT DtpM converting holomycin to thiolutin.[9] Similarly, the XRD MT is neither encoded within the NRPS nor as a separate enzyme within the XRD BGC[10] (Figure 1b).

Here, we identified and characterized the amide *N*-MT XrdM that is encoded outside of the XRD gene cluster using proteomic analysis, MT-candidate screening, gene deletion, and allied approaches. We further showed that XrdM and DtpM are isofunctional enzymes toward XRDs and holomycin. X-ray crystal structures, molecular modeling, site-directed mutagenesis and kinetic activity assays allowed for a thorough comparison of XrdM and DtpM in terms of structure and activity.

Results

Identification of the XRD MT XrdM

Since our previous study revealed the MT involved in XRD methylation to be *S*-adenosyl methionine (SAM)-dependent,[10] we screened the *Xenorhabdus doucetiae* genome for all the SAM-dependent MTs and found 60 candidates (Figure 1c, Table S2). 45 of them were excluded based on their presence and high sequence identity (cutoff > 60 %) to proteins encoded in *Xenorhabdus* species that do not carry the XRD BGC[11] (Table S2) or methylate any of the XRD derivatives (Figure S2). The remaining 15 MT candidates were considered to be specific for *X. doucetiae* and therefore selected for further experiments (Figure 1c, Table S2).

Notably, a previously generated △*hfq* mutant, in which the gene encoding Hfq (an RNA chaperone mediating mRNA/sRNA interaction) is deleted, is characterized by a strong decrease in most natural products including XRDs (Figure S3).[12] When we exchanged the natural promoter of the NRPS gene *xrdA* with an arabinose inducible promoter, the resulting strain △*hfq* P_{BAD}_*xrdA* (Table S3) produced mostly non-methylated XRDs (XRD-243, −271, and −299) with only trace amounts of methylated XRD-271Me, whereas in wild type (WT) *N*-methylated XRDs (XRD-243Me, −271Me, and −299Me) were the main derivatives (Figure S3). These findings imply that the transcription and/or translation of both XRD BGC and the corresponding XRD MT is down-regulated in the △*hfq* mutant in comparison to

WT, making △*hfq* P_{BAD}_*xrdA* an ideal host for the overexpression of selected MT candidates. In the following, we separately overexpressed the 15 MT candidates in *X. doucetiae* △*hfq* P_{BAD}_*xrdA* and analyzed the strains for the production of (non−)methylated XRDs (Figure 2a and Figure S4). In parallel, we did a comparative proteomic analysis between △*hfq* and WT *X. doucetiae* strains and could show that among the selected 15 MT candidates, four of them, referred to as MT3, MT13, MT14, and MT15, were down-regulated in △*hfq* (Figure 1d and Figure S5). These four down-regulated MTs were individually selected for gene knockouts in WT *X. doucetiae* and probed for the production of (non−)methylated XRDs (Figure 2b). Both experimental approaches, that is overexpression and knock-out studies, revealed that MT3, located 592 kb away from the XRD BGC, was the only MT capable of catalyzing the conversion of non-methylated XRDs to *N*-methylated XRDs, and therefore was named XrdM (Xenorhabdin methyltransferase) (Figure S1c).

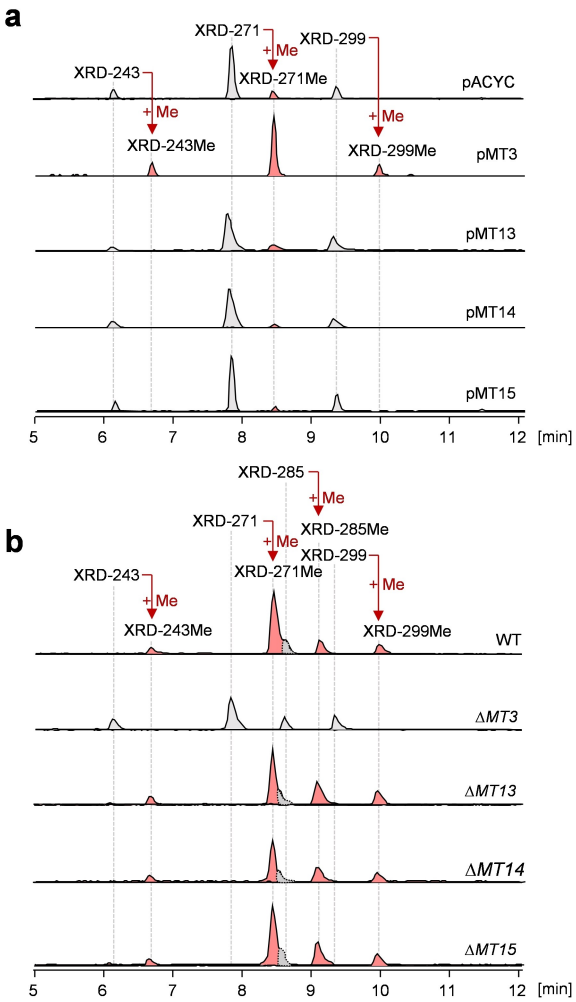

Figure 2. Extracted ion chromatograms (EIC) of XRDs from plasmid expression strains (**a**) and gene-deletion strains (**b**) (representative of biological triplicates). Peaks referring to non-methylated XRDs and *N*-methylated XRDs are colored in grey and red, respectively. pACYC represents the mutant △*hfq* P_{BAD}_xrdA containing an empty plasmid pACYC (see details in Table S3), serving as a control for strains carrying pMT3, 13, 14, and 15, respectively. Results of other MT expression strains are shown in Figure S4.

XrdM and DtpM are Isofunctional Enzymes

Recently, DtpM from *Saccharothrix algeriensis* NRRL B-24137 was shown to *N*-methylate holomycin and numerous DTP derivatives.[9] Notably, a BLASTP search against the genome of *X. doucetiae* using DtpM as a query did not reveal XrdM but rather MT15 (Figure S6, 32 % sequence identity) as the closest homolog, which however proved to be inactive against XRDs (Figure 2). Furthermore, the closest sequence homolog of XrdM in the holomycin producer *S. algeriensis* NRRL B-24137 was not DtpM but CTG1_5739 (Figure S7). To get an overview of the similarities between XrdM and DtpM, we generated a sequence similarity network (SSN). This analysis revealed the close association of DtpM with a number of phenolic-*O*-MTs (e.g., LaPhzM,[13] CrmM,[14] AzicL,[15] and CalO6[16]) and several *N*-MTs (e.g., WelM[17]) belonging to the Pfam00891 family (Figure S8). In contrast, XrdM did not cluster with those enzymes but with other MTs of the Pfam13649 family and some Pfam13847 MTs (Figure S8). Therefore, in terms of sequence analysis, XrdM (246 amino acids) and DtpM (353 amino acids) can be considered as unrelated methyltransferases (14.6 % sequence identity, Figure S9).

However, considering that the substrates of XrdM and DtpM, XRDs and holomycin, differ only in the length of their acyl side chain, we surmised that both enzymes might have some cross reactivity. To test this hypothesis, we generated a holomycin-producing *X. doucetiae* strain (*Δhfq ΔxrdE::hlmA* P_{BAD}_*xrdA*) by replacing the XRD specific acyltransferase gene *xrdE* with the gene *hlmA* encoding the acetyltransferase for holomycin biosynthesis in *S. clavuligerus* ATCC 27064[2] (details in Figure S10 and S11). Since expression of pXrdM in this holomycin producing strain (*Δhfq ΔxrdE::hlmA* P_{BAD}_*xrdA* pXrdM) yielded thiolutin (Figure S10), and expression of pDtpM in the XRD producing strain *Δhfq* P_{BAD}_*xrdA* generated methylated XRDs (Figure S10), XrdM and DtpM are isofunctional despite their sequence differences.

Structural Comparison of XrdM : SAH and DtpM : SAH

To investigate the structural basis for this isofunctionality of XrdM and DtpM, we purified (Figure S12) and crystallized both enzymes. In the following, X-ray structures of XrdM and DtpM in complex with the cofactor S-adenosylhomocysteine (SAH) were solved to 2.1 Å and 1.75 Å resolution, respectively (Figure S13, Figure S14 and Table S9).

The structure of XrdM is similar to many other MTs, but most related to ToxA, a dual-specificity *N*-MT that catalyzes the last two steps of toxoflavin biosynthesis and that shares a sequence identity of 54.3 % with XrdM[18] (Table S10 and Figure S15a, c). Like ToxA, XrdM is a monomer in solution (Figure S12a),[18] folding into two subdomains. The larger N-

terminal domain features the canonical Rossmann motif GxGxxG which is highly conserved across class I SAM-dependent MTs.[18–19] The smaller C-terminal domain is known as the flap domain[18] and its three anti-parallel β-strands build large parts of the substrate binding pocket. At the interface of both domains a pronounced cofactor- and substrate-binding cleft is located (Figure S13a). The surface charge distribution indicates a polar environment around the cofactor with more hydrophobic portions at the putative ligand binding site (Figure S13b). As the N-terminus (residues 4–23) is disordered in the crystal structure, the substrate binding cleft is accessible to artificial dimer contacts in the crystal lattice (Figure S13a, c), thereby blocking the active site of the enzyme.

Like XrdM, DtpM adopts a two-domain fold with the active site in between (Figure S14b), but the topology is different. DtpM features a pronounced N-terminal, helical domain that mediates homodimerization and substrate binding, while the C-terminal domain comprises the Rossmann fold (GxGxG motif) (Figure S14d and Figure S16a). The structure of DtpM is related to various class I *O*-MTs[20] with the phenazine *O*-MT LaPhzM from *Lysobacter antibioticus* being the closest relative (PDB 6C5B, Table S11 and Figure S16).[13] DtpM forms a homodimer (Figure S12c) that is considered to be stable in solution (interface area of 3670.8 Å^2)[21] and that is probably functionally relevant, as the N-terminus of each subunit contributes to the substrate binding pocket of the other (Figure 3b and Figure S17a). The active site of DtpM is shielded from the solvent and is rather negatively charged (Figure S14c). Most interestingly however, DtpM and its active site surroundings are, apart from the Rossmann fold, exclusively made of helices, while XrdM uses three antiparallel β-sheets and one helix to shape the XRD binding site (Figure S14d).

In conclusion, although both XrdM and DtpM are class I MTs for the same substrates sharing the typical Rossman fold, their oligomeric states and substrate binding domains are different. To understand how the unrelated active site architectures mediate the same substrate scope, we aimed for ligand complex structures with both XrdM and DptM.

Modeling of Product-Bound XrdM and Mutagenesis

Since the packing of XrdM crystals prevented the determination of experimental ligand complex structures and since the N-terminus (residues 4–23) of XrdM, which was disordered in the crystal structure, is crucial for catalytic activity (see mutant ΔNterm, Figure 4c) similar as for ToxA (Figure S15c-e),[18] we conducted in silico modeling of XrdM with SAH and XRD-271Me using the ToxA structure[18] (Figure S15a–e) and the full-length XrdM AlphaFold2[22] prediction.

The model of product-bound XrdM indicates that the DTP scaffold is recognized by hydrogen bonds with Tyr7, Tyr14, Gln23 (indirectly), His115, Tyr116, and His238 (indirectly) (Figure 3a), while hydrophobic contacts provided by Tyr18, Phe112, Ala145, Leu161, Phe179, Phe189 and Met237 anchor both the DTP core as well as the acyl side chain (Figure 3a and Figure S15b). To validate the modeling, we selected key amino acids (Tyr7, Tyr14, Tyr18, Gln23, Phe112, His115, Tyr116 and His238, Figure 3a) for mutagenesis and tested the mutant proteins for their activity in qualitative LC–MS assays (Figure 4c). Selected mutants were then further analyzed in quantitative luminescence-based kinetic experiments[23] (Figure 4d and Figure S18).

The XrdM mutants H238A (5-fold increase of K_M, 2.5-fold reduction of k_{cat}) and Q23A (7-fold increase of K_M, 5-fold reduction of k_{cat}) had moderately reduced catalytic activity and parameters compared to WT XrdM (Figure 4c, d and Figure S18). This observation agrees with the model in which His238 and Gln23 hydrogen bond via a water molecule to the amide oxygen atom of the aliphatic tail of XRD-271Me (Figure 3a). Next, we mutated Tyr18 and Phe112, which are suggested to stack laterally and from top to the disulfide moiety of XrdM-271Me (Figure 3a). The catalytic activity of the Y18A mutant was slightly impaired compared to WT (2.5-fold increase of K_M, 5-fold decrease of k_{cat}), whereas substrate turnover of the F112A variant was more severely affected (Figure 4c, d and Figure S18). Due to the apparently lower substrate affinity (8-fold increase of K_M) and impaired catalysis (33-fold reduction of k_{cat}), catalytic efficiency of the F112A mutant was 320 times lower compared to WT XrdM (Figure 4d and Figure S18). To evaluate the impact of an aromatic versus an aliphatic side chain, we additionally evaluated the F112L mutant and found that it was fully active (Figure 4c). In conclusion, hydrophobic but not necessarily aromatic amino acids at position 112 mediate important interactions with the dithiolopyrrolone ring that are crucial for the catalytic activity of XrdM. Notably, in ToxA, Trp112 stacks from top to the substrate, but whether its function can be replaced by an aliphatic amino acid as well has not been tested (Figure S15d).[18]

Next, we investigated the impact of Tyr14. Both Y14F and Y14A mutants were evaluated for their activity toward XRD. While the Y14A variant was hardly functional (Figure 4c), the Y14F version was active, but 192 times less than WT XrdM (Figure 4d and Figure S18). In fact, the Y14F mutant was compromised in both K_M (4.3 times increased) and k_{cat} (50 times reduced) (Figure 4d and Figure S18). These results imply that the aromatic character of Tyr14 is essential for efficient catalysis, but its hydroxyl group additionally supports substrate binding and conversion.

To probe the relevance of the hydrogen bonds provided by Tyr7, His115 and Tyr116 for substrate turnover, the XrdM variants Y7A, Y7F, H115A and Y116F were created. The Y7A variant appeared inactive under the tested conditions (Figure 4c), while the Y7F mutant retained significant catalytic activity (Figure 4c). Detailed kinetic analysis revealed that the K_M value of XrdM-Y7F was almost unchanged (increased by 1.5-fold), but k_{cat} was 25-fold reduced (Figure 4d). Hence, similar to Tyr14, both the aromatic character of Tyr7 as well as its ability to hydrogen bond to the DTP scaffold are essential for efficient substrate conversion. These results agree with studies on ToxA, reporting modest and strong reductions of ToxA activity for the mutations Y7F and Y7A, respectively.[18] Similarly, it has

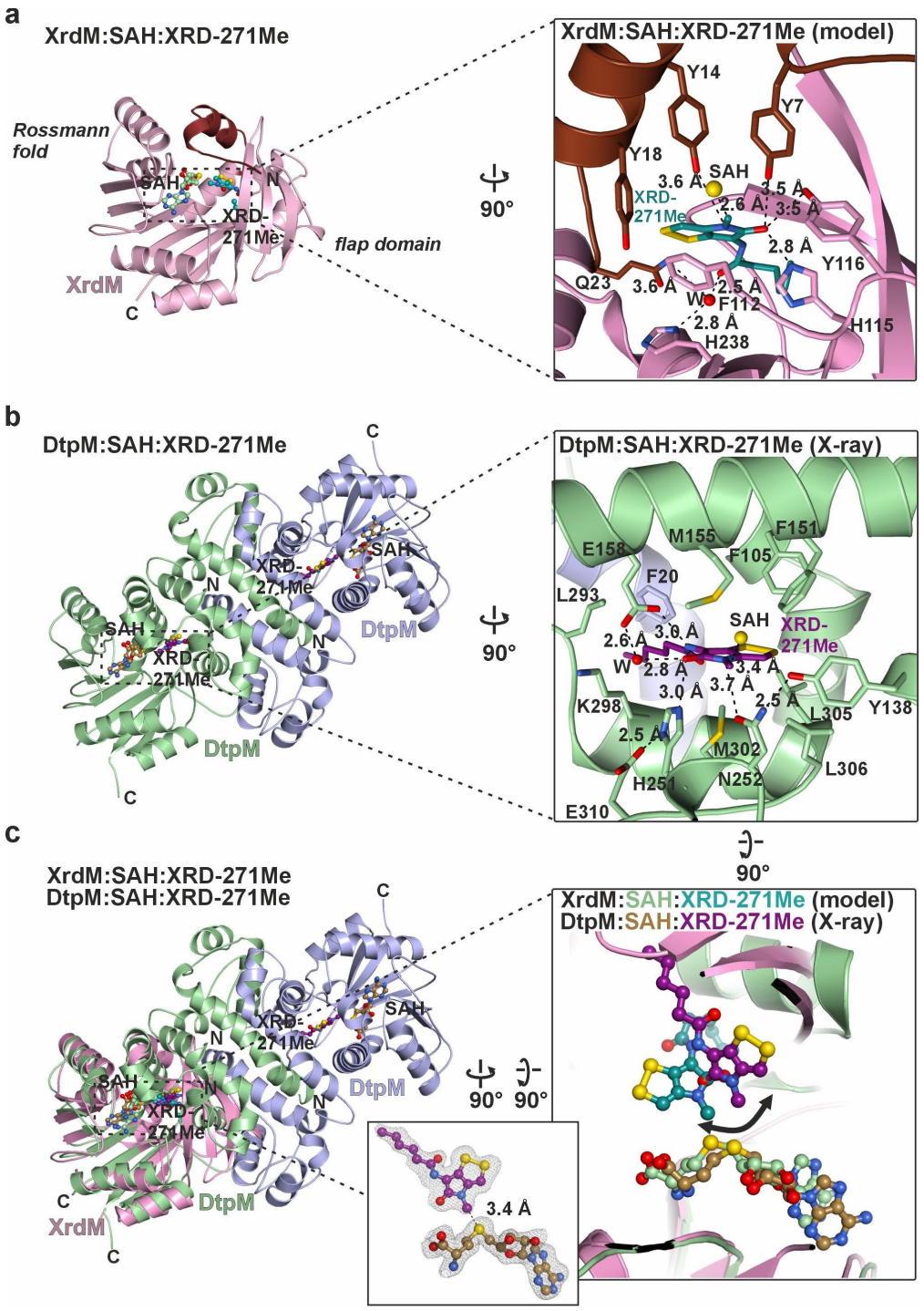

Figure 3. Ligand binding to XrdM and DtpM. **a**) Left: Ribbon illustration of the in silico modeling of the XrdM:SAH:XRD-271Me complex. Since the N-terminal residues 4–23 of XrdM (dark red), which are essential for catalytic activity (see mutant ΔNterm, Figure 4c), were not resolved in the X-ray structure (Figure S13a), the AlphaFold2 model of XrdM was used for modeling. SAH and XRD-271Me are shown as multicolored ball-and-stick models; N- and C-termini are labeled. Right: Zoom-in at the active site of XrdM with XRD-271Me shown in teal. Amino acid residues required for ligand binding or catalysis are labeled by the one-letter code and numbered. Black dotted lines indicate predicted hydrogen bond interactions. Distances are given. W (red sphere) indicates a water molecule that contributes to ligand coordination. Only the sulfur atom of SAH is shown (yellow sphere). **b**) Left: X-ray structure of dimeric DtpM (ribbon illustration) with bound SAH and XRD-271Me (multicolored ball-and-sticks-models); N- and C-termini are labeled. For substrate-bound DtpM structure see Figure S17. Right: Zoom-in at the active site of DtpM with XRD-271Me shown in purple. The active site structure differs significantly from that of XrdM (panel a). Labeling and illustration according to panel a. **c**) Left: Superposition of product-bound XrdM (modeling data) and DtpM (X-ray data) ribbon illustrations. While XrdM and DtpM share the Rossmann fold, their substrate binding domains are unrelated in secondary and tertiary structure. Right: In consequence ligand recognition at the active site is different (compare right panels **a**, **b** and the superposition of both in (**c**). Of note, XRD-271Me is flipped by 120° in DtpM compared to XrdM. Small zoom-in window: experimental $2F_O$-F_C omit electron density map for DtpM bound SAH and XRD-271Me contoured to 1σ.

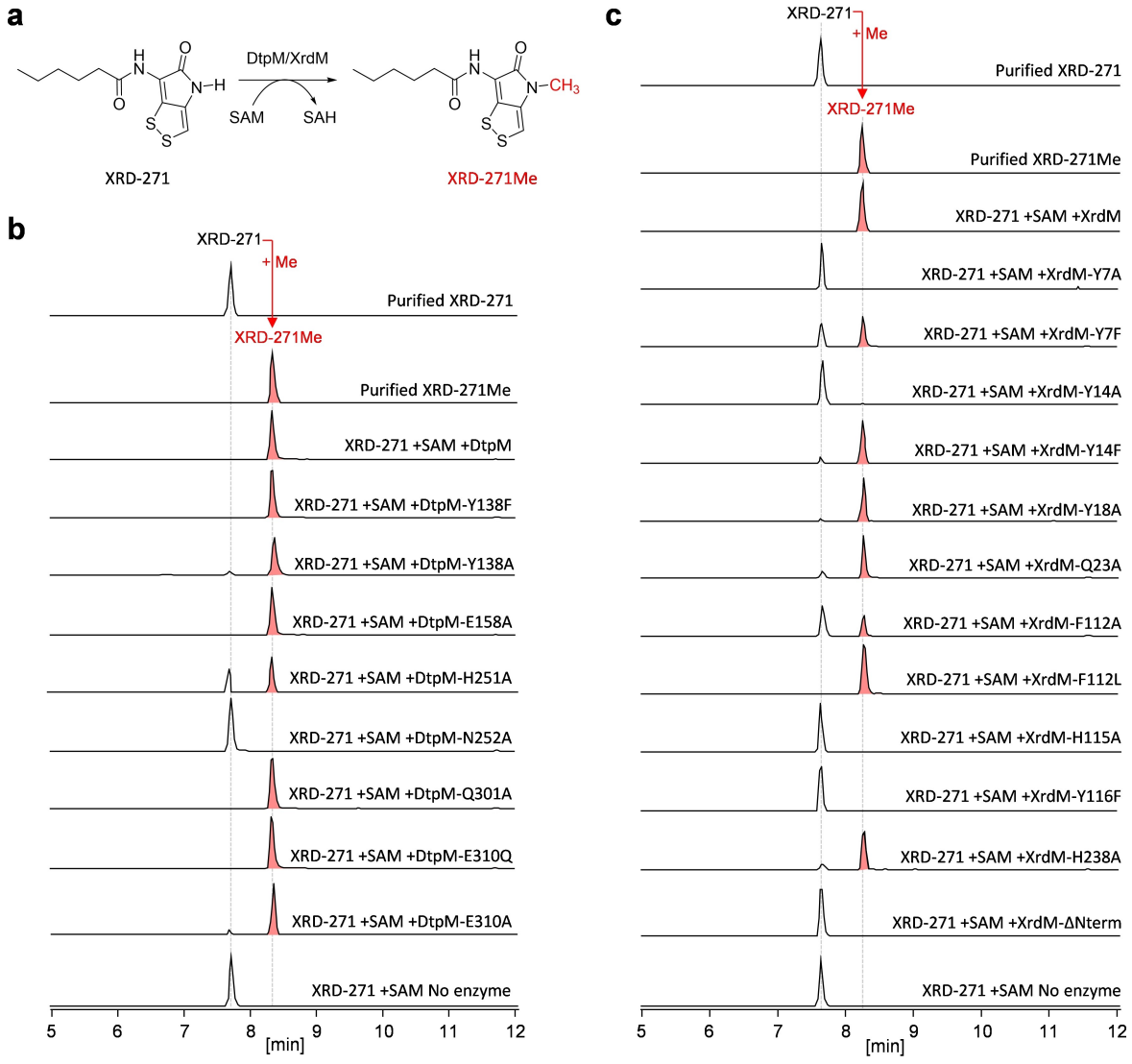

d

	DtpM	DtpM-Y138F	DtpM-Y138A	DtpM-H251A	DtpM-N252A
K_M (μM)	3 ± 1	6 ± 4	17 ± 8	85 ± 49	24 ± 7
k_{cat} (min^{-1})	0.4 ± 0.08	0.3 ± 0.08	0.04 ± 0.008	0.06 ± 0.03	0.1 ± 0.01 (× 10^{-2})
k_{cat}/K_M (10^4 $\mu M^{-1}min^{-1}$)	1577 ± 373	613 ± 181	22 ± 4	7 ± 2	0.5 ± 0.1

	DtpM-E310A	XrdM	XrdM-Y7F	XrdM-Y14F	XrdM-Y18A
K_M (μM)	13 ± 7	6 ± 2	9 ± 4	26 ± 14	15 ± 3
k_{cat} (min^{-1})	0.2 ± 0.05	0.1 ± 0.02	0.4 ± 0.08 (× 10^{-2})	0.2 ± 0.07 (× 10^{-2})	0.02 ± 0.002
k_{cat}/K_M (10^4 $\mu M^{-1}min^{-1}$)	135 ± 28	192 ± 34	5 ± 1	1 ± 0.2	15 ± 2

	XrdM-Q23A	XrdM-F112A	XrdM-H115A	XrdM-Y116F	XrdM-H238A
K_M (μM)	42 ± 18	48 ± 32	56 ± 16	10 ± 3	29 ± 18
k_{cat} (min^{-1})	0.02 ± 0.006	0.3 ± 0.2 (× 10^{-2})	0.6 ± 0.1 (× 10^{-3})	0.2 ± 0.01 (× 10^{-4})	0.04 ± 0.01
k_{cat}/K_M (10^4 $\mu M^{-1}min^{-1}$)	6 ± 0.8	0.6 ± 0.1	0.11 ± 0.01	0.02 ± 0.005	14 ± 4

Figure 4. Activity assays of DtpM, XrdM and their mutants. **a**) Methylation reaction of XRD-271 to XRD-271Me catalyzed by DtpM and XrdM. **b**) Qualitative LC–MS based activity assay of WT or mutant DtpM after incubation for 30 min. Purified XRD-271 and XRD-271Me were used as standards (shown on the top). The reaction mixture without enzyme served as a negative control (shown at the very bottom). The EIC peaks are representative of two replicates. **c**) Qualitative LC–MS based activity assay of wild type or mutant XrdM after incubation for 30 min according to panel b. **d**) Kinetic data for the methylation of XRD-271 catalyzed by DtpM, XrdM, and their mutants as derived from the raw data shown in Figure S18. The kinetic assay was carried out in triplicates.

been noted for ToxA that residues Asn115 and Tyr116, corresponding to His115 and Tyr116 of XrdM, are in hydrogen bonding distance to the substrate[18] (Figure 3a). Consistently, the XrdM mutants H115A and Y116F showed

drastically reduced catalytic activity (1745 times for H115A and 9600 times for Y116F) (Figure 4c, d and Figure S18). While K_M was increased 9.5-fold for H115A and 1.7-fold for Y116F, k_{cat} was severely decreased for both (167 times for H115A and 5000 times for Y116F), suggesting that the two residues are of key importance for substrate activation and turnover.

Together, these data imply that His115, Tyr116, Tyr7 and Tyr14 are catalytically important residues of XrdM. Considering that the residues 1–23 are disordered in the experimentally solved apo XrdM structure, we propose that they form a flexible lid to the active site. Notably, the catalytic importance and conservation of two tyrosine residues – one as part of the mobile N-terminal segment (Tyr7 in XrdM) and a second Tyr (Tyr116 in XrdM) at the active site – has been noted before for other *N*-MTs such as ToxA (Figure S15d) and glycine *N*-MT.[18,24]

Substrate- and Product-Bound Structures of DtpM as well as Mutagenesis

Co-crystallization trials with DtpM, SAH and either XRD-271 or XRD-271Me led to substrate- (2.2 Å resolution, Table S9, Figure S17a) and product-bound structures (1.75 Å resolution, Table S9, Figure 3b). Compared to apo DtpM, the experimental electron density maps did not show any conformational changes (Figure S17c) but clearly visualized SAH and the respective ligand at the active site (Figure 3b, Figure S17a). Furthermore, XRD-271 and XRD-271Me bind identically to DtpM (Figure S17c). The distance between the sulfur atom of SAH and the acceptor nitrogen atom in XRD-271 (3.8 Å, Figure S17a) is ideal for the alkylation reaction. By modeling SAM instead of SAH into the DtpM:XRD-271 active site, the angle connecting the sulfur atom of SAH, the methyl group to be transferred and the acceptor nitrogen atom of XRD-271 was found to be 166° and thus close to the linear arrangement supposed for a S_N2 methyl transfer.[25]

Superposition of the Rossmann folds of product-bound XrdM and DtpM illustrates similar binding of the cofactor SAH but a 120° flip for XRD-271Me in DtpM compared to XrdM (Figure 3c), implying that the two enzymes evolved different ways to recognize the same ligand. This observation is underpinned when analyzing the enzyme-ligand interactions at the amino acid level. The core ring structures of XRD-271 and XRD-271Me are stabilized in DtpM by numerous hydrophobic amino acid residues (e.g. Phe105, Phe151, Met155, Leu293, Met302, Leu305 and Leu306) (Figure 3b, Figure S17a). The aliphatic tail of XRD-271/XRD-271Me is outstretched and points into a deep hydrophobic channel that extends to the protein surface. Specifically, the DtpM amino acid side chains Leu293, Val297, Lys298 as well as Gln301 mediate Van-der-Waals contacts with the XRD-tail (Figure S17b). In addition, Phe20 and Arg23 from the neighboring DtpM monomer contribute non-polar contacts to this binding site (Figure 3b, Figure S17b). Based on the pronounced depth of the channel, substrate derivatives with longer or shorter aliphatic tails (e.g. holomycin with its shorter acetyl side chain) than that of XRD-271 are likely to fit as well.

Besides the hydrophobic interactions, several hydrogen bonds help recognizing XRD-271(Me) and presumably also holomycin. Gln301 for example may weakly hydrogen bond to the amide oxygen atom of the side chain of XRD-271(Me) (Figure S17b). In addition, Glu158 hydrogen bonds directly to the nitrogen atom of the same amide and indirectly via a water molecule to the amide oxygen atom of the DTP moiety (Figure 3b and Figure S17b). Mutation of Gln301 or Glu158 to alanine did however not affect DtpM activity in a qualitative LC–MS assay (Figure 4b), suggesting that these two interactions are not decisive.

We next investigated the polar interaction between the target nitrogen atom of XRD-271(Me) and Asn252 as well as indirectly Tyr138 (Figure 3b, Figure S17a). Based on the LC–MS and kinetic activity assays, the Y138F mutant retained high activity (Figure 4b, d), excluding a key function of the hydroxyl group in substrate activation. The aromatic character of Tyr138 appears to be more important, as the corresponding Y138A mutant was reduced in its catalytic efficiency by 72-fold compared to WT (5.7-fold increase of K_M and 10-fold decrease of k_{cat}; Figure 4b, d). Most likely Tyr138 of DptM serves the same function as Tyr14 of XrdM. By contrast, the DtpM variant N252A was hardly catalytically active (3154-fold drop in catalytic efficiency; Figure 4b, d). Considering the position of Asn252 relative to XRD-271 in the crystal structure and the catalytic parameters of the N252A mutant (8-fold increase of K_M, 400-fold reduction of k_{cat} compared to WT, Figure 4d, Figure S18), Asn252 most likely activates the target nitrogen for methyl transfer.

Finally, the relevance of the hydrogen bond network between His251 and Glu310 for substrate binding and activation was probed. Three mutants, E310Q, E310A and H251A, were tested by LC–MS and kinetic activity assays. While the E310Q mutant was not compromised (probably because substitution of the side-chain carboxylate for an amide retains the hydrogen bonding pattern with His251), the E310A variant was 11.7 times and the H251A mutant 225-fold less active than the WT enzyme (Figure 4b, d). This data is in agreement with a previous kinetic analysis of DtpM, showing that the mutations E310A and H251A cause a reduction in catalytic efficiency by a factor of 41 and 643, respectively.[9] The discrepancy in numbers might arise from the different substrates used in the enzymatic assays. We here tested the activity of DptM towards XRD-271, while the previous kinetic data[9] were collected on holomycin as a substrate. Altogether, the residues Asn252 and His251 as well as to a minor extent Glu310 are important for DtpM activity and also conserved in DtpM-related *O*-MTs[9] such as LaPhzM.[13]

In summary, XrdM and DtpM differ in terms of quaternary structure, fold and size of the substrate binding domain as well as ligand coordination, recognition and activation (Figure 3). For instance, XrdM and DtpM bind their substrate in different orientations relative to the cofactor (Figure 3c) and although both activate their substrates by hydrogen bonds to the amide oxygen atom next to the

methylation site in the DTP ring, they employ different residues to do so. XrdM uses two tyrosines (Tyr7 and Tyr 116) and a histidine (His115) side chain, while DtpM engages a histidine (His251) and to a minor extent glutamate (Glu310). Moreover, DtpM uses Asn252 to directly hydrogen bond the acceptor nitrogen atom for methyl transfer, whereas, in XrdM, Tyr14 takes over this function.

Implications for XrdM and DtpM-Related Methyltransferases

Strikingly, many tested sequence homologs of XrdM (e.g. MT4, MT13, MT14, CTG1_5739 and ToxA, Figure S19c) and DtpM (MT15) do not methylate XRDs (Figure 2a, Figure S5 and Figure S10). We therefore compared the sequences and structures of XrdM and ToxA. Considering that ToxA naturally methylates an azapteridine scaffold with no extensions, one could speculate that the aliphatic tail of XRD-271 might be too large to fit into the ToxA active site. In this regard, the ToxA residues Val145 and Leu237 could pose some steric hindrance to XRD-271 binding. Next, we inspected the sequences and AlphaFold2 predictions for the XrdM homologs MT4, MT13 and MT14, and looked for residues that are involved in XRD-271 binding or activation in XrdM but missing in all three homologous MTs (Figure S19a, b). We identified that Tyr18 is replaced by Ser in MT4, MT13 and MT14. Mutation of Ser18 to Tyr in MT13 and MT14 however did not activate these MTs toward XRD-271 (Figure S19c). In addition to Tyr18, MT4 lacks other key residues like His115, Tyr116 and His238. However, even the MT4 quadruple mutant S18Y-C115H-H116Y-D238H did not convert XRD-271 (Figure S19c), suggesting that other factors like altered geometries, dynamics or charge distributions at the active site might be relevant. We thus conclude that the failure to explain the inactivity of MT4, MT13 and MT14 toward XRD-271 might result from both technical limitations (resolution of X-ray structure/accuracy of the in silico modeling and the AlphaFold2 algorithm regarding side chain conformations[26]) as well as the inability to predict activities and substrate specificities from primary or tertiary protein structures.

Conclusion

Our study showcases a natural product, DTP, whose core skeleton is synthesized by a conserved NRPS protein in different species, but is methylated at the final stage by two isofunctional methyltransferases, XrdM and DtpM. Here, we characterized these two enzymes and showed that they are completely unrelated in terms of sequence, structure and ligand binding. Phylogenetic classification of DtpM and XrdM homologs (Figure S20) suggests that XrdM and DtpM tend to be specific to Gram-negative and Gram-positive bacteria, respectively, fitting the notion that most natural product methyltransferases are tailored for a specific biosynthesis within a certain clade or species.[19a] Considering the common interest in engineering and designing methyltransferases for biocatalytic applications,[19a,27] the two protein scaffolds of XrdM and DptM might represent promising starting points for directed evolution approaches to create novel DTP derivatives as potential anti-infectives.

Additional information

There are 3 Supplementary files accompanying this manuscript: 1) Supporting Information (Figures S1–S20, and Tables S1–S11); 2) Extended_Excel_sheet_1; 3) Extended_Excel_sheet_2.

Acknowledgements

Work in the Bode Group was supported by an ERC Advanced Grant (835108) and the Max-Planck-Society. E.M.H. and M.G. acknowledge financial support by the DFG – SFB 1309–325871075. We thank the staff of the beamline X06SA at the Paul-Scherrer-Institute, Swiss Light Source, Villigen Switzerland for assistance during data collection. The research leading to these results has received funding from the European Community's Seventh Framework Programme (FP7/2007-2013) under BioStruct-X (grant agreement N°283570). We are grateful to K. Gärtner for technical assistance and to the students F. Reinhardt, V. Gebler and M. Hofberger for experimental support. Open Access funding enabled and organized by Projekt DEAL.

Conflict of Interest

The authors declare no competing interests.

Data Availability Statement

Protein coordinates have been deposited in the RCSB Data Bank under the accession codes 8RDL (XrdM:SAH), 8RDM (DptM:SAH), 8RDN (DptM:SAH:XRD-271), 8RDO (DtpM:SAH:XRD-271Me).

Keywords: biosynthesis · dithiolopyrrolone natural products · post-NRPS methylation · structural biology · enzyme catalysis

[1] B. Li, W. J. Wever, C. T. Walsh, A. A. Bowers, *Nat. Prod. Rep.* **2014**, *31*, 905–923.
[2] B. Li, C. T. Walsh, *Proc. Natl. Acad. Sci. USA* **2010**, *107*, 19731–19735.
[3] Z. Qin, S. Huang, Y. Yu, H. Deng, *Mar. Drugs* **2013**, *11*, 3970–3997.
[4] a) B. Oliva, A. O'Neill, J. M. Wilson, P. J. O'Hanlon, I. Chopra, *Antimicrob. Agents Chemother.* **2001**, *45*, 532–539; b) B. V. McInerney, R. P. Gregson, M. J. Lacey, R. J. Akhurst, G. R. Lyons, S. H. Rhodes, D. R. Smith, L. M. Engelhardt, A. H. White, *J. Nat. Prod.* **1991**, *54*, 774–784.
[5] K. M. J. de Mattos-Shipley, C. Greco, D. M. Heard, G. Hough, N. P. Mulholland, J. L. Vincent, J. Micklefield, T. J. Simpson,

C. L. Willis, R. J. Cox, A. M. Bailey, *Chem. Sci.* **2018**, *9*, 4109–4117.
[6] K. J. Labby, S. G. Watsula, S. Garneau-Tsodikova, *Nat. Prod. Rep.* **2015**, *32*, 641–653.
[7] Y. Y. Zhang, N. Shao, W. H. Wen, G. L. Tang, *Org. Lett.* **2022**, *24*, 127–131.
[8] a) D. H. Scharf, A. Habel, T. Heinekamp, A. A. Brakhage, C. Hertweck, *J. Am. Chem. Soc.* **2014**, *136*, 11674–11679; b) E. R. Duell, M. Glaser, C. Le Chapelain, I. Antes, M. Groll, E. M. Huber, *ACS Chem. Biol.* **2016**, *11*, 1082–1089.
[9] X. Chen, R. M. Johnson, B. Li, *ACS Catal.* **2023**, *13*, 1899–1905.
[10] E. Bode, A. O. Brachmann, C. Kegler, R. Simsek, C. Dauth, Q. Zhou, M. Kaiser, P. Klemmt, H. B. Bode, *ChemBioChem* **2015**, *16*, 1115–1119.
[11] N. J. Tobias, H. Wolff, B. Djahanschiri, F. Grundmann, M. Kronenwerth, Y. M. Shi, S. Simonyi, P. Grün, D. Shapiro-Ilan, S. J. Pidot, T. P. Stinear, I. Ebersberger, H. B. Bode, *Nat Microbiol* **2017**, *2*, 1676–1685.
[12] E. Bode, A. K. Heinrich, M. Hirschmann, D. Abebew, Y. N. Shi, T. D. Vo, F. Wesche, Y. M. Shi, P. Grün, S. Simonyi, N. Keller, Y. Engel, S. Wenski, R. Bennet, S. Beyer, I. Bischoff, A. Buaya, S. Brandt, I. Cakmak, H. Çimen, S. Eckstein, D. Frank, R. Fürst, M. Gand, G. Geisslinger, S. Hazir, M. Henke, R. Heermann, V. Lecaudey, W. Schäfer, S. Schiffmann, A. Schüffler, R. Schwenk, M. Skaljac, E. Thines, M. Thines, T. Ulshöfer, A. Vilcinskas, T. A. Wichelhaus, H. B. Bode, *Angew. Chem. Int. Ed. Engl.* **2019**, *58*, 18957–18963.
[13] J. Jiang, D. Guiza Beltran, A. Schacht, S. Wright, L. Zhang, L. Du, *ACS Chem. Biol.* **2018**, *13*, 1003–1012.
[14] Y. Zhu, P. Fu, Q. Lin, G. Zhang, H. Zhang, S. Li, J. Ju, W. Zhu, C. Zhang, *Org. Lett.* **2012**, *14*, 2666–2669.
[15] Y. Ogasawara, H.-w. Liu, *J. Am. Chem. Soc.* **2009**, *131*, 18066–18068.
[16] O. V. Tsodikov, C. Hou, C. T. Walsh, S. Garneau-Tsodikova, *BMC Struct. Biol.* **2015**, *15*, 13.
[17] M. L. Hillwig, H. A. Fuhrman, K. Ittiamornkul, T. J. Sevco, D. H. Kwak, X. Liu, *ChemBioChem* **2014**, *15*, 665–669.
[18] M. K. Fenwick, B. Philmus, T. P. Begley, S. E. Ealick, *Biochemistry* **2016**, *55*, 2748–2759.
[19] a) D. K. Liscombe, G. V. Louie, J. P. Noel, *Nat. Prod. Rep.* **2012**, *29*, 1238–1250; b) P. Laurino, Á. Tóth-Petróczy, R. Meana-Pañeda, W. Lin, D. G. Truhlar, D. S. Tawfik, *PLoS Biol.* **2016**, *14*, e1002396.
[20] Q. Sun, M. Huang, Y. Wei, *Acta Pharm. Sin. B* **2021**, *11*, 632–650.
[21] E. Krissinel, K. Henrick, *CompLife 2005* **2005**, *3695*, 163–174.
[22] J. Jumper, R. Evans, A. Pritzel, T. Green, M. Figurnov, O. Ronneberger, K. Tunyasuvunakool, R. Bates, A. Zidek, A. Potapenko, A. Bridgland, C. Meyer, S. A. A. Kohl, A. J. Ballard, A. Cowie, B. Romera-Paredes, S. Nikolov, R. Jain, J. Adler, T. Back, S. Petersen, D. Reiman, E. Clancy, M. Zielinski, M. Steinegger, M. Pacholska, T. Berghammer, S. Bodenstein, D. Silver, O. Vinyals, A. W. Senior, K. Kavukcuoglu, P. Kohli, D. Hassabis, *Nature* **2021**, *596*, 583–589.
[23] K. Hsiao, H. Zegzouti, S. A. Goueli, *Epigenomics* **2016**, *8*, 321–339.
[24] a) Y. Takata, Y. Huang, J. Komoto, T. Yamada, K. Konishi, H. Ogawa, T. Gomi, M. Fujioka, F. Takusagawa, *Biochemistry* **2003**, *42*, 8394–8402; b) S. G. Lee, Y. Kim, T. D. Alpert, A. Nagata, J. M. Jez, *J. Biol. Chem.* **2012**, *287*, 1426–1434.
[25] E. Abdelraheem, B. Thair, R. F. Varela, E. Jockmann, D. Popadic, H. C. Hailes, J. M. Ward, A. M. Iribarren, E. S. Lewkowicz, J. N. Andexer, P. L. Hagedoorn, U. Hanefeld, *ChemBioChem* **2022**, *23*, e202200212.
[26] T. C. Terwilliger, D. Liebschner, T. I. Croll, C. J. Williams, A. J. McCoy, B. K. Poon, P. V. Afonine, R. D. Oeffner, J. S. Richardson, R. J. Read, P. D. Adams, *Nat. Methods* **2023**.
[27] a) A. Kunzendorf, B. Zirpel, L. Milke, J. P. Ley, U. T. Bornscheuer, *ChemCatChem* **2023**, *15*, e202300951; b) X. Wu, M. Yuwen, Z. Pu, Z. Zhao, H. Yu, J. Zha, *Appl. Microbiol. Biotechnol.* **2023**, *107*, 1663–1672; c) T. R. Valentic, J. T. Payne, C. D. Smolke, *ACS Catal.* **2020**, *10*, 4497–4509.

Manuscript received: June 7, 2024
Accepted manuscript online: August 26, 2024
Version of record online: ■■, ■■

Research Article

Enzyme Catalysis

L. Su, +. M. Huber, M. Westphalen, J. Gellner, E. Bode, T. Köbel, P. Grün, M. M. Alanjary, T. Glatter, K. Cirnski, R. Müller, D. Schindler, M. Groll,* H. B. Bode* e202410799

Isofunctional but Structurally Different Methyltransferases for Dithiolopyrrolone Diversification

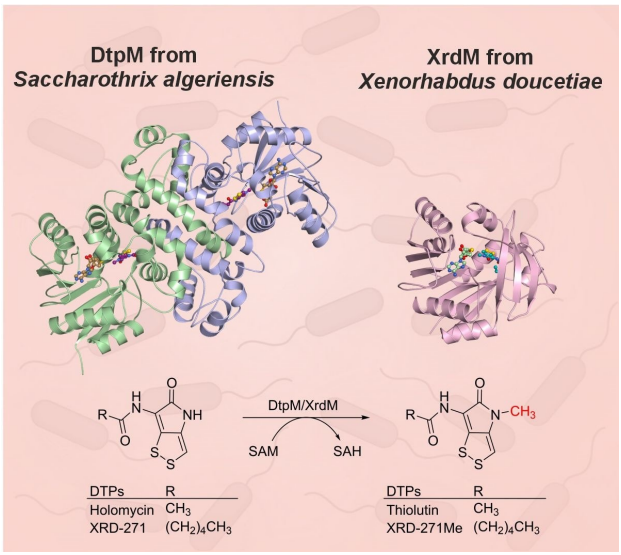

Two for one job: DtpM and XrdM are two bacterial enzymes that have different structures but still catalyze the same reaction: the amide *N*-methylation of dithiolopyrrolones (DTPs). Ligand binding to both enzymes was studied using X-ray crystallography, modeling, mutagenesis and activity assays. The results suggest that different organisms developed distinct methyltransferases for the same task by convergent evolution.